Observation of energy transfer at optical frequency to an ultrathin silicon waveguide

Liping Fang,[1,*] lefteris danos,[2] tom markvart,[3,4] Rui chen[1,*]

[1]Department of Electrical and Electronic Engineering, Southern University of Science and Technology, Shenzhen 518055, China
[2]Department of Chemistry, Energy Lancaster, Lancaster University, Lancaster LA1 4YB, UK
[3]Centre for Advanced Photovoltaics, Czech Technical University, Prague 16627, Czech Republic
[4]Solar Energy Laboratory, Faculty of Engineering and Physical Sciences, University of Southampton, Southampton SO17 1BJ, UK
*Corresponding author: liping.fang@outlook.com, chenr@sustech.edu.cn

Energy transfer from a submonolayer of rhodamine 6G molecules to a 130 nm thick crystalline silicon waveguide is investigated. The dependence of fluorescence lifetime of rhodamine on its distance to the silicon waveguide is characterized and modeled successfully by a classical dipole model. The energy transfer process could be regarded as photon tunneling into the silicon waveguide via the evanescent waves. The experimental observed tunneling rate is well described by an analytical expression obtained via complex variable analysis in the complex wavenumber plane. © 2020 Optical Society of America

Energy transfer between organic light absorber and proximal inorganic semiconductor such as silicon (Si) is attracting the attention of researchers recently [1, 2]. The joint merits of organic and inorganic materials offer the possibility to fabricate optoelectronic devices with unprecedented properties [3]. The incident radiation on the organic absorber could be funneled into the inorganic material via energy transfer. Energy transfer at optical frequencies to an ultrathin Si waveguide has been investigated theoretically previously [4]. However, experimental observation of such a process has yet to be reported. In this letter, we demonstrate energy transfer from a submonolayer of rhodamine 6G molecules to the underlying ultrathin Si waveguide via time-resolved fluorescence studies.

As shown in Fig. 1, all the samples (size of 15 mm×15 mm) were fabricated on a silicon-on-insulator (SOITECH) substrate. The thickness of the Si device layer and the silicon dioxide (SiO₂) box layer was 130±5 nm and 1934±5 nm, respectively. Variable thickness spacer layer between rhodamine and the Si device layer was SiO₂ film deposited by plasma-enhanced chemical vapor deposition (PECVD, Oxford Instruments PlasmaPro80). The rhodamine submonolayer was obtained by spin-coating of a few drops of dilute alcohol solution of rhodamine 6G (3×10^{-4} mol/L) on

the substrate with the speed of 3000 round per minute for 60 seconds [5, 6]. To improve the stability of rhodamine [7], a final capping layer of polymethyl methacrylate (PMMA) with thickness around 70 nm was deposited on all the samples by spin-coating of a few drops of 2% anisole solution of PMMA (MicroCHEM NANO 950PMMA). The thickness and refractive index of the SiO₂ spacer layer and the PMMA capping layer were characterized by spectroscopic ellipsometry using a Horiba UVISEL phase-modulated ellipsometer. PMMA was chosen due to its similar refractive index with the SiO₂ spacer layer in the concerned spectral range, thereby providing a homogeneous optical environment for the rhodamine molecules.
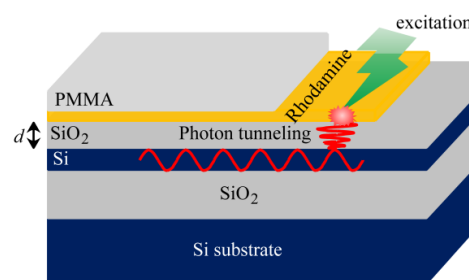

Fig. 1. Sample structure of energy transfer from submonolayer rhodamine to an ultrathin silicon waveguide.

Fluorescence lifetime was measured by a time-resolved fluorescence spectrometer (PicoQuant FluoTime 300) which employed the time-correlated single photon counting (TCSPC) technique. The excitation source was a 512 nm diode laser (PicoQuant LDH-P-C-520) working at 40 MHz repetition rate. Fluorescence emission was collected by a high numerical aperture collecting lens, passed through a 532 nm long-pass edge filter (Semrock LP03-532RE-25) and captured by a single photon detector module (PicoQuant PMA-C 192-N-M) equipped with a grating monochromator (Bentham MSH300). This monochromator was set at 600 nm, i.e. fluorescence emission was

monitored at this wavelength to avoid reabsorption or inter-molecular energy transfer, which would complicate the analysis of energy transfer to Si. Fluorescence decay curves were collected by TCSPC via the TimeHarp 260 module. The obtained decays were fitted with the sum of two exponential functions after deconvolution of the instrument response function (IRF), which was obtained by measuring the scattering decay curve of the pulsed laser at the excitation wavelength. The longer lifetime was attributed to rhodamine, whereas the shorter one (1.1±0.5 ns, similar for all rhodamine-Si distance) was attributed to PMMA [7]. Chance, Prock and Silbey (CPS) developed a classical model for molecular fluorescence near interface [8]. The excited fluorescent molecules were modeled as forced and damped electric dipoles. The normalized damping rate (inverse fluorescence lifetime) of an electric dipole emitting near a single interface is given by:

$$\hat{b}_{\text{VED}} = q \, \text{Re} \left(\frac{3}{2k_1^3} \int_0^\infty dk_\rho \frac{k_\rho^3}{k_{1x}} \left\{ r_{12}^{\text{TM}} \exp(i2k_{1x}d) + \frac{1}{q} \right\} \right) \quad \textbf{(1)}$$

$$\hat{b}_{\text{HED}} = q \, \text{Re} \left\{ \begin{array}{l} \frac{3}{4k_1^3} \int_0^\infty dk_\rho k_{1x} k_\rho \left\{ -r_{12}^{\text{TM}} \exp(i2k_{1x}d) + \frac{1}{q} \right\} + \\ \frac{3}{4k_1^3} \int_0^\infty dk_\rho \frac{k_\rho}{k_{1x}} \left\{ r_{12}^{\text{TE}} \exp(i2k_{1x}d) + \frac{1}{q} \right\} \end{array} \right\} \quad \textbf{(2)}$$

where $\hat{b}_{\text{VED}}$ and $\hat{b}_{\text{HED}}$ represent the damping rate of a vertical electric dipole (VED) and a horizontal electric dipole (HED), respectively, normalized to the damping rate without the presence of the interface. q is the fluorescence quantum yield of the molecule, k_ρ and k_{ix} are the in and out of plane wavenumbers in region i and defined by $k_i^2 = k_\rho^2 + k_{ix}^2$, d is the distance between the dipole and the interface, r_{12}^{TE} and r_{12}^{TM} are the Fresnel reflection coefficients for the transverse electric (TE) and transverse magnetic (TM) waves at the interface between region 1 and region 2, respectively. For dipole emission near a thin waveguide, these two reflection coefficients are given by Airy's summation:

$$r = \frac{-r_{21} + r_{23}e^{i2\phi}}{1 - r_{21}r_{23}e^{i2\phi}} \quad \textbf{(3)}$$

where r_{ij} represents the Fresnel reflection coefficient for the TE/TM waves at the interface between region i and region j, $\phi = k_{2x}t$ the phase retardation for light travelling through the thin waveguide with thickness t. For an isotropic distribution of dipole orientations, the damping rate is given by $\hat{b}_{\text{VED}} = (\hat{b}_{\text{VED}} + 2\hat{b}_{\text{HED}})/3$.

The dependence of fluorescence lifetime of rhodamine on its distance to the Si waveguide surface is illustrated in Fig. 2. The measured fluorescence lifetime can be well fitted by the CPS model for a HED, i.e. Eq. (2), using the following refractive index for Si and SiO₂: $n_1 = n_3 = n_{\text{SiO}_2} = 1.458$, $n_2 = n_{\text{Si}} = 3.940+0.020i$ [9]. The horizontal dipole orientation for rhodamine 6G molecules rest on flat substrates has been revealed by previous angular fluorescence intensity [10] and fluorescence lifetime investigations [11].
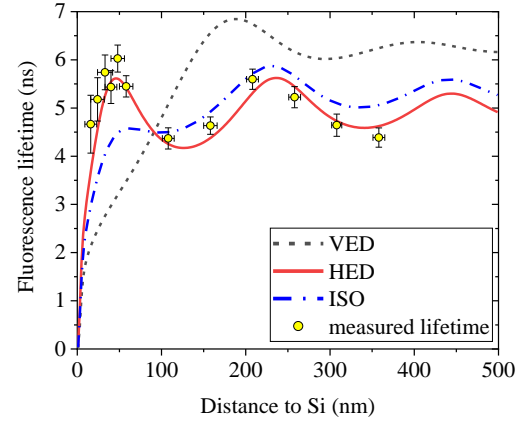

Fig. 2. Comparison of fluorescence lifetime with CPS model for different dipole orientation configurations.

Ford and Weber [12] introduced a power spectrum $d\mathscr{P}/dk_\rho$ to define the total power $\mathscr{P}$ dissipated by the dipole emitter via $\mathscr{P} = \int_0^\infty dk_\rho (d\mathscr{P}/dk_\rho)$. Since $\mathscr{P}$ is the product of photon energy and the dipole damping rate, $d\mathscr{P}/dk_\rho$ is directly proportional to the integrand of the dipole damping rate given by Eq. (1) or Eq. (2). The radiated power in the far field can be obtained by integrating $d\mathscr{P}/dk_\rho$ in the range $0 < k_\rho < k_{10}$. The power transferred to Si can be calculated in the range $k_{10} < k_\rho < k_{20}$. Note that this part of energy is evanescent in region 1, but propagating in region 2. We have termed this process "photon tunneling", through the potential barrier which confines photons inside the high refractive index material by total internal reflection [13].
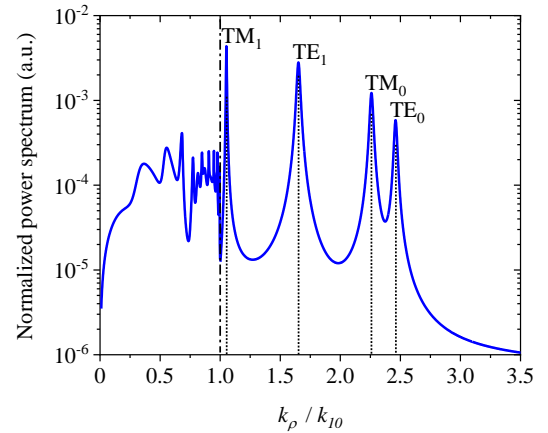

Fig. 3. Power spectrum of a HED emitting near the silicon waveguide.

The power spectrum of a HED emitting near the structure shown in Fig. 1 is plotted in Fig. 3. There are four distinct peaks in the range $k_\rho > k_{10}$. We find that these peaks correspond to the waveguide modes supported by the Si waveguide, after we solved the dispersion relation (as shown in Fig. 4) of the structure shown in Fig. 1 numerically.
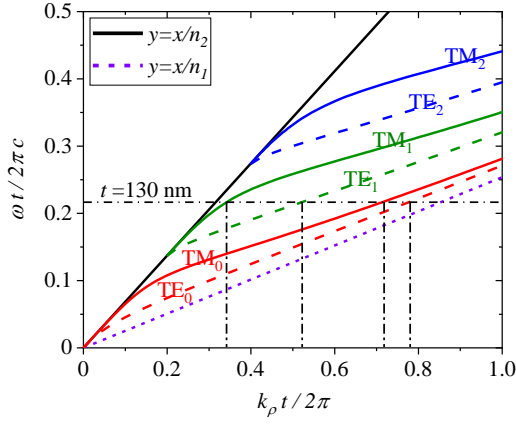
Fig. 4. Dispersion relation of the silicon waveguide.

Fig. 5. Comparison of modeled and observed photon tunneling rates.

It is apparent that Eq. (3) has singularities when the denominator approaches zero. These singularities (slightly off the real axis) are the poles in the complex plane of the in-plane wavenumber, which physically corresponds to the waveguide modes supported by the Si waveguide. Analytical expressions were obtained to approximate the tunneling rate to these modes. We first expand the denominator of Eq. (3) in the vicinity of the related pole in the complex in-plane wavenumber plane, then perform contour integral along a semicircle with radius approaching zero around that pole. The photon tunneling rate for VED and HED are found to be:

$$\hat{b}_{VED}^{pt} \approx \sum_{m=0}^{M} \frac{3\pi}{2k_1^3} \frac{k_{\rho m}^3}{|k_{1xm}|} \frac{g_{TM}(k_{\rho m})}{f_{TM}(k_{\rho m})} \exp(-2|k_{1xm}|d) \quad (4)$$

$$\hat{b}_{HED}^{pt} \approx \sum_{m=0}^{M} \frac{3\pi}{4k_1^3} |k_{1xm}| k_{\rho m} \frac{g_{TM}(k_{\rho m})}{f_{TM}(k_{\rho m})} \exp(-2|k_{1xm}|d)$$
$$+ \sum_{m=0}^{N} \frac{3\pi}{4k_1} \frac{k_{\rho m}}{|k_{1xm}|} \frac{g_{TE}(k_{\rho m})}{f_{TE}(k_{\rho m})} \exp(-2|k_{1xm}|d) \quad (5)$$

where M and N are the number of TM and TE modes supported by the waveguide, g_{TM} and f_{TM} are given by

$$g_{TM}(k_\rho) = \frac{4\varepsilon_1\varepsilon_2 |k_{1x}| k_{2x}}{\varepsilon_2^2 |k_{1x}|^2 + \varepsilon_1^2 k_{2x}^2} \quad (6)$$

$$f_{TM}(k_\rho) = 2k_\rho \left\{ \frac{t}{k_{2x}} + \frac{\varepsilon_1\varepsilon_2 \left(|k_{1x}|^2 + k_{2x}^2\right)}{\varepsilon_1^2 |k_{1x}| k_{2x}^3 + \varepsilon_2^2 |k_{1x}|^3 k_{2x}} + \frac{\varepsilon_3\varepsilon_2 \left(|k_{3x}|^2 + k_{2x}^2\right)}{\varepsilon_3^2 |k_{3x}| k_{2x}^3 + \varepsilon_2^2 |k_{3x}|^3 k_{2x}} \right\} \quad (7)$$

where ε_i is the dielectric constant of region i, omitting which in Eqs. (6) and (7), yields g_{TE} and f_{TE}. The tunneling rate given by Eq. (5) is calculated numerically and compared with the observed tunneling rate (obtained by subtracting the far field emission rate into the total damping rate) in Fig. 5. The solid curves signify the contribution of each waveguide mode. It is depicted that the modeled tunneling rate fits well with the observed data.
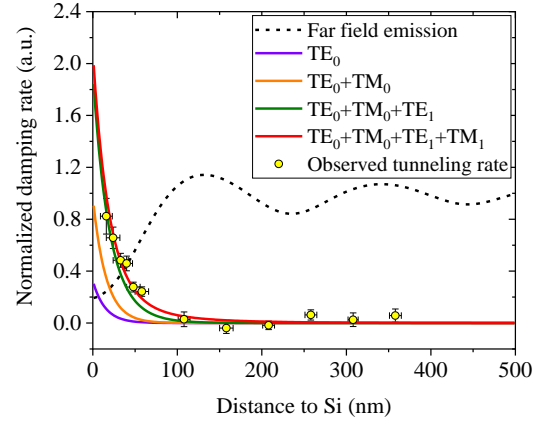
Energy transfer from a molecular emitter to an ultrathin Si waveguide is demonstrated in this work. The excited molecules transfer their excitonic energy to the underlying Si waveguide via photon tunneling. This is different from the Förster-type resonance energy transfer, which is only observed for emitter-Si distances less than 5 nm [1, 2]. Through a complex variable analysis, analytical expressions have been found to successfully approximate the observed tunneling rates. The above experiments and theoretical analysis are important to the design and optimization of hybrid optoelectronic devices based on energy transfer.

Disclosures. The authors declare no conflicts of interest.

References

1. N. Alderman, L. Danos, L. Fang, M. C. Grossel, and T. Markvart, Chem. Commun. **53**, 12120 (2017).
2. L. Danos, N. R. Halcovitch, B. Wood, H. Banks, M. P. Coogan, N. Alderman, L. Fang, B. Dzurnak, and T. Markvart, Faraday Discuss., (2020).
3. W. Peng, S. M. Rupich, N. Shafiq, Y. N. Gartstein, A. V. Malko, and Y. J. Chabal, Chem. Rev. **115**, 12764 (2015).
4. B. J. Soller, H. R. Stuart, and D. G. Hall, Opt. Lett. **26**, 1421 (2001).
5. T. F. Heinz, C. K. Chen, D. Ricard, and Y. R. Shen, Phys. Rev. Lett. **48**, 478 (1982).
6. W. P. Ambrose, P. M. Goodwin, J. C. Martin, and R. A. Keller, Phys. Rev. Lett. **72**, 160 (1994).
7. L. Gaudreau, K. J. Tielrooij, G. E. D. K. Prawiroatmodjo, J. Osmond, F. J. G. de Abajo, and F. H. L. Koppens, Nano Lett. **13**, 2030 (2013).
8. R. R. Chance, A. Prock, and R. Silbey, Adv. Chem. Phys. **37**, 1 (1978).
9. M. A. Green, Sol. Energy Mater. Sol. Cells **92**, 1305 (2008).
10. H. Sano, G. Mizutani, and S. Ushioda, Surf. Sci. **223**, 621 (1989).
11. G. Cnossen, K. E. Drabe, and D. A. Wiersma, J. Chem. Phys. **98**, 5276 (1993).
12. G. W. Ford, and W. H. Weber, Phys. Rep. **113**, 195 (1984).
13. L. Fang, K. S. Kiang, N. P. Alderman, L. Danos, and T. Markvart, Opt. Express **23**, A1528 (2015).